ACS Sustainable Chemistry & Engineering

Article

Waste driven Bio-Carbon Electrode Material for Na-ion Storage Applications

Mullaivananathan Vadivazhagan, Packiyalakshmi Parameswaran, Ulaganathan Mani, and Kalaiselvi Nallathamby

ACS Sustainable Chem. Eng., **Just Accepted Manuscript** • DOI: 10.1021/acssuschemeng.8b02199 • Publication Date (Web): 09 Sep 2018

Just Accepted

ACS Publications

is published by the American Chemical Society. 1155 Sixteenth Street N.W., Washington, DC 20036

Waste driven Bio-Carbon Electrode Material for Na-ion Storage Applications

*Mullaivananathan Vadivazhagan[#], Packiyalakshmi Parameswaran[#], Ulaganathan Mani[#] and Kalaiselvi Nallathamby**

[#]Electrochemical Power Systems Division, CSIR- Central Electrochemical Research Institute, Karaikudi- 630 003, Tamil Nadu, India

*Corresponding author E-mail: kalaiselvicecri@gmail.com

ABSTRACT: Corn silk is a waste material obtained from corn that contains carbohydrates, proteins and vitamins. Interestingly, corn silk derived carbon (CSC) after activation is found to possess larger specific surface area (2550 $m^2 g^{-1}$) and appreciable pore volume (0.95 $cm^3 g^{-1}$). In the present investigation, CSC electrodes are used to fabricate symmetric coin and pouch-cells individually and investigated for electrochemical performance in half and full cell assembly systematically. Half-cell performance of CSC exhibits a maximum specific capacity of 256 mA h g^{-1} at 100 mA g^{-1}. The subsequently assembled symmetric coin type sodium-ion capacitor (SIC) delivers a maximum specific capacitance of 126 F g^{-1} at 0.3 A g^{-1} and the pouch-cell delivers 135 F g^{-1} at the same current density. Symmetric capacitors are found to withstand high current densities up to ~3 A g^{-1} with nominal capacitance values, thus qualifying the suitability of CSC for SIC applications. A maximum specific energy of ~109 Wh kg^{-1} and a power of ~12.16 kW kg^{-}

[1] have been realized from the symmetric SICs. Feasibility of the fabricated devices for practical application has been demonstrated by glowing LEDs and by running a clock for 25 minutes.

KEYWORDS: Corn silk derived carbon, Sodium-ion capacitor, Biomass, Supercapacitor, EDLC

INTRODUCTION

In recent years, electrochemical energy storage technology is receiving worldwide attention due to the emerging demand on huge electrical energy usage in various applications ranging from toys to electric vehicles (EVs). Based on the storage mechanism involved, electrochemical energy storage devices are classified as batteries and supercapacitors. While batteries are known to provide high energy, supercapacitors offer high power. Among the various class of supercapacitors, lithium (LIC) and sodium ion capacitors (SIC) are promising energy storage devices for application in electric vehicles (EVs) and hybrid electric vehicles (HEVs). In the case of LIC, high cost of the electrode materials and the low abundance of lithium on the earth's crust are the critical issues. On the other hand, sodium is one of the most abundant elements on the earth's crust bestowed with low cost and environmental benignity advantages [1-4]. Hence, SICs assume importance as alternative and competitive technology to replace LICs. In addition, storage of sodium ions is faster than lithium ions due to the large size and thus exhibits higher power than LICs[5]. In other words, SICs are known to offer high energy and power density along with good cycle life in practical applications. Generally, SICs are fabricated in different configurations, namely, symmetric and asymmetric or hybrid capacitor, in which Na salt containing solution is used as the electrolyte medium. Thus, the electrolyte plays the role of Na^+ ion conducting medium as well as the source of Na^+ ions. In the case of symmetric configuration, two identical EDLC or

pseudo-capacitive type electrodes are used[6-7]. On the other hand, hybrid SIC system involves the combination of two different electrodes such as EDLC type of electrode (Activated carbon) on one side and battery type of electrode (mostly battery anode materials) on the other side[3, 8]

Basically, non-aqueous (sodium salt containing organic electrolyte) SIC exhibits higher energy density than that of aqueous SIC. Herein, organic electrolytes offer wide operating potential window, typically in the range of above 2.5 V, which in turn helps to enhance the energy density compared with those of aqueous electrolytes. In addition, in the case of organic electrolytes, one can use cheaper current collectors such as Cu or Al, which is yet another valuable point to choose organic electrolyte for the current study[9]. However, organic electrolytes are known to contain larger solvated ions and exhibit low dielectric constant, which in turn poses limitations on the specific capacitance of carbonaceous electrode materials deployed in supercapacitors. However, it is well known that the specific capacitance of carbon depends on various other factors such as specific surface area, pore size and distribution of pores associated with the sample[10]. In this direction, biomass derived carbons fulfill the above requirements more readily and their electrochemical properties are being extensively studied by various research groups for their multifarious applications, including energy storage devices[4, 11-21].

Besides the larger specific surface area with desirable pore size and distribution, EDLC performance enhances due to the pseudo-capacitive behavior of carbon based materials. i.e., fast redox reactions occurring on the surface functionalities (such as oxygen, nitrogen and phosphorous) of carbon are responsible for the pseudo-capacitive behavior[17, 22-26]. Interestingly, the stability of psudeocapacitance behavior arising from surface functionalities of carbon is appreciable in organic electrolytes than in aqueous electrolytes[9]. Recently, Yang et.al.[27] based on their study on sisal fiber derived carbon in LIC (Lithium ion capacitor) with lithium salt containing

organic electrolyte reported that apart from the presence of larger specific surface area of carbon, the amount of hetero atoms (O and N) also plays a significant role in realizing appreciable capacitance behavior. However, presence of higher concentration of hetero atoms is also reported to exhibit inferior rate capability behavior due to the increasing limitations experienced against the faster diffusion of ions resulting from the decomposition of electrolyte. In other words, superior rate capability behavior could generally be attributed to the hierarchical porosity and the presence of lower content of hetero atoms. In addition, the pre-lithiated electrodes can provide increased cycling stability of LICs to the extent of more than 100000 cycles with high specific energy. However, it involves safety issues for large scale applications due to the usage of lithium powder and hence is not very popular[28-29]. Recently, Kim et.al.[6] have stated that citrus peel derived carbon in SIC system (sodium salt containing organic electrolyte) could store sodium ions electrostatically and sodium ions that are chemisorbed on the surface of C-O, C-N and C=O functional groups also involve in the storage mechanism due to the pseudo capacitive nature. As a result, such a citrus peel derived carbon based symmetric SIC is shown to deliver a specific capacitance of 110 F g^{-1} at 0.1 A g^{-1}.

In the context of exploitation of biomass derived carbons for energy storage applications, Corn silk derived carbon (CSC) is demonstrated for its potential electrode behavior in SIC through this work. It is well known that corn silk is a bio-waste material, originating from the cultivated corn. This harmless, potential bio-waste is largely available not only in India but also in countries like China, the United States, France, etc. Corn silk contains proteins, carbohydrates and vitamins that act as the source of carbon and nitrogen in many applications and more precisely, in the field of medicine [30-31]. Recently, N, P and Fe doped corn silk derived carbon has been demonstrated for its electrocatalytic behavior in zinc-air batteries[32]. On the other hand, carbon derived from corn silk

and activated further with simple KOH has been deployed as active electrode material in SIC and the storage mechanism as a function of variable potential window has been investigated in the present study. It is noted that the as-prepared CSC qualifies itself as a suitable electrode material for sodium ion storage, due to its high specific surface area (2550 $m^2 g^{-1}$), larger pore volume (0.95 $cm^3 g^{-1}$), uniform pore size distribution and the presence of nitrogen functional group that leads to the excellent electrochemical performance by accommodating more number of sodium ions to facilitate the required electrochemical behavior.

RESULTS AND DISCUSSION

Physical characterization of CSC

Figure 1 describes the schematic to synthesise corn silk derived carbon (CSC) by using simple KOH activation. The precursor of corn silk is initially subjected to pre-carbonization, followed by KOH activation to obtain the activated carbon for investigation as an electrode for sodium storage.

XRD pattern of CSC synthesized at 800° C is shown in figure 2 (a). Presence of two broad peaks at 2Θ = 23.6 and 43.6° could be assigned to (002) and (001) crystallographic planes of graphite respectively. The presence of such broad peaks indicates the amorphous behavior of CSC and the possible presence of randomly oriented graphene like sheets. The calculated d-spacing value, corresponding to the (002) plane of CSC is 0.386 nm, which is higher than that of pure graphitic carbon (0.335 nm), and helps to accommodate more number of sodium ions[33]. Figure S1 shows the XRD pattern of corn silk heated at 350° C temperature, which is denoted as CS-350. It displays two broad peaks at 2Θ = 23.6 and 43.6°, corresponding to (002) and (001) planes respectively. In addition, we could observe impurity peaks (figure S1) due to the presence of calcium, which is matching with the JCPDS pattern of calcium (00-010-0348). Interestingly, peaks due to calcium

are not found in the case of KOH activated CSC (figure 2), thereby confirming the removal of calcium due to HCl wash upon activation.

Further, Raman spectrum of CSC is shown in figure 2b, which helps to understand the perfect or imperfect and disordered arrangement of atoms in the carbon structure, as evident from the I_D/I_G ratio. In figure 2b, two peaks are located at 1335 and 1580 cm^{-1}, corresponding to the presence of defect and disordered structure in the graphene layers of carbon materials (D band) and the vibration of sp^2 bonded carbon atoms in a 2D-hexagonal lattice (G band)[34-35]. The calculated I_D/I_G ratio of CSC (from Raman spectrum) is 1.04, which evidences the presence of disordered and amorphous nature of carbon[36].

Morphology at different stages of corn silk upon activation has been investigated using scanning electron microscope (SEM), which is shown in figure S2. Figure S2 (a-c) shows the SEM images of washed, dried and crushed corn silk powder. In addition, Figure S2 (d-g) and (h-j) correspond to the pre-carbonized and the final product of CSC. Herein, we could observe that the pre-carbonized form of corn silk retains the morphology of dried corn silk powder. But in the case of activated carbon, we can observe changes in the morphology compared with its initial stage. Such a change could be attributed to the high alkaline pH level of KOH as well as the activation temperature deployed during the process of KOH activation, which leads to morphological change. Such an observation is not unusual, as we have similar reports in the literature[37-39].

The morphology of CSC was investigated further using Field Emission Scanning Electron Microscopy (FESEM) and High Resolution Transmission Microscopy (HRTEM), which are shown in figure 3 (a-f). One can observe the sheet like structure of CSC from the captured two-dimensional images (Figure 3 (a-e)). In addition, Figure 3 (a-b) reveals the arrangement of graphene like sheets with the desirable random orientation. Figure 3 (c-e) further evidences the

uniform distribution of pores resulting from KOH activation, as identified from the presence of dark spots. Finally, SAED pattern of CSC shown in figure 3f confirms the amorphous nature of carbon, from the ring pattern.

EDAX analysis of CS-350 and activated CSC (shown in figure S3 (a-b)) evidences the presence of elements in the compound. Non activated CS-350 contains C (64.99 %), N (22.3 %), O (10.17 %), Ca (2.37 %), Si (0.1 %), S (0.04 %), Mg (0.02 %) and Al (0.01 %) elements and the activated CSC contains only C (89.37 %), O (9.14 %), and N (1.49 %). Absence of other elements in the activated CSC is due to the leaching process carried out by using HCl wash during KOH activation. Further, EDAX analysis evidences the presence of calcium in CS-350 which in turn substantiates the XRD observations.

XPS analysis helps to determine the presence of elements and bonding groups in CSC. The XPS spectrum of CSC is shown in figure 4(a-d), which displays the corresponding scan of carbon, oxygen and nitrogen main peaks located at 284.8, 533.1 and 400.4 eV respectively. Deconvoluted spectrum of C1s scan (figure 4b) shows three peaks at 284.8, 286.2 and 289.2 eV, corresponding to the presence of C-C, C-O and –COOH functional groups. Figure 4c shows the deconvoluted spectrum of O1s spectrum that contains two different peaks located at 533.17 and 533.7 eV, corresponding to C-OH and O-C=O groups respectively[40]. Similarly, N1s scan (Figure 4d) shows a peak at 400.4 eV, representing the presence of graphitic nitrogen[35]. Further, electrical conductivity of CSC measured using the four probe technique is 16.05 mS cm^{-1}, as evident from the response of current vs. voltage behaviour, shown in figure S5.

Further, to understand the porosity behavior and the details of surface area related properties of CSC, BET analysis was done. Figure 4e shows the nitrogen adsorption-desorption isotherm of CSC that reveals the presence of type-I isotherm, which is due to the microporous nature of carbon.

The BET surface area of KOH activated corn silk derived carbon is 2550 m^2 g^{-1}. In addition, BJH pore size distribution shown in figure 4f indicates that the pore size of CSC is found in the range of 1.95 nm and the pore volume is 0.95 cm^3 g^{-1}. The observed larger specific surface area, microporous nature of carbon and the larger pore volume helps in improving the electrochemical storage behavior of CSC electrode. N_2 adsorption/desorption isotherm of CS-350 is measured and shown in the figure S4, displays the presence of Type II isotherm, corresponding to the presence of non-porous or macro porous behavior of CS-350. Further, the pore size and pore volume have been evaluated from the BJH method (inset of figure S4). The calculated average pore size is 30 Å (3 nm) and the pore volume is 0.04 cm^3 g^{-1}. Comparison of the obtained BET parameters of CS-350 with activated CSC is discussed in Table S1. From the table, one can understand the importance of activation in terms of increased surface area, reduced pore size and increased pore volume of CSC, which are desirable for an electrode to exhibit better electrochemical performance. Subsequently, we measured the tap density value of CSC by manual tapping method [41]. 0.367 g (2 ml) of CSC was placed in a 5 ml measuring jar and tapped for 1000 times manually. Then we measured the tapped volume of CSC and from its mass, we calculated the tap density. The calculated tap density of CSC is 0.6 g cm^{-3}. The obtained lower tap density is due to the presence of larger surface area of CSC [42-43].

Electrochemical studies of CSC electrode in sodium storage

Half-cell configuration of CSC electrode has been investigated in the potential window between 1.5 and 4.2 V *vs.* Na/Na^+ by using sodium metal as the counter and reference electrode and in presence of 1M of $NaClO_4$ dissolved in EC:PC (1:1 v/v) solution. Figure 5a shows the cyclic voltammogram of CSC electrode in the voltage range of 1.5 to 4.2 V at various scan rates (2, 5 and 10 mV s^{-1}). As we know, when the potential surpasses the OCV of the cell (2.7 V *vs.* Na), it

will respond to only adsorption /desorption of anions present in the electrolyte. Therefore, the anion, *viz.* ClO_4^- will be adsorbed/desorbed during cycling in the present case and is evident from the quasi-rectangular CV curve (Figure 5a). This implies that the energy storage behaviour occurrs at this potential window (above OCV) is mainly due to non-Faradic reaction mechanism. In other words, the storage mechanism involved here is solely due to the electric double layer capacitive (EDLC) behavior. Hence, the reaction mechanism associated with the surface of CSC electrode that does not obey the diffusion controlled process could be understood. Further, presence of small humps in the oxidation and reduction potentials (*viz.* around ~2 V) is due to the sodium ion adsorption occurring at the surface of the functional groups associated with CSC in the form of C-O, C-N and C=O[6]. Further, CV curves are found to retain their shape even at high scan rates (10 mV s^{-1}), thereby indicating the acceptable electrochemical stability of the CSC electrode.

Galvanostatic cycling behavior of CSC electrode was investigated in the potential window of 1.5-4.2 V at different current densities and the result is furnished in figure 5(b-d). When the CSC half-cell is cycled at the rate of 1 A g^{-1} for 1000 cycles (figure 5b), it delivers an initial capacity of 60 mA h g^{-1} and at the 1000th cycle, an acceptable capacity of 44 mA h g^{-1} is obtained, which is comparable with the reported behavior [6]. Retention of capacity observed at the 1000th cycle, upon comparison with the initial cycle is found to be more than 70 %, which in turn substantiates the appreciable stability of the currently chosen CSC electrode material. It is noted that the CSC electrode shows a maximum specific capacity of 256 mA h g^{-1} at a tested current density of 0.1 A g^{-1}. Similarly, the cell delivers a specific capacity of 212, 159, 126, 84 and 53 mA h g^{-1} over the studied cycle range at 0.2, 0.5, 1, 2 and 5 A g^{-1}, respectively and the corresponding rate capability performance is appended in figure 5c. Notably, the cell delivers a specific capacity of 35 mA h g^{-1} for the maximum current density of 10 A g^{-1}. These obtained storage capacity

values of the cells are mainly due to the sodium ion adsorption/desorption occurring on the surface of CSC electrode and the observed values are superior than the previously reported values[44-45]. Capacity *vs.* voltage behaviour of CSC based half-cell at different current rates is shown in figure 5d. From the plot, it is observed that the charge and discharge behavior of the cell shows a linear variation with the cell voltage which in turn reveals the occurrence of EDLC behavior associated with the surface of CSC electrode. In order to evaluate the full cell performance of the CSC electrodes in a device, various cell architectures such as coin and flexible symmetric pouch cell were fabricated. A coin type symmetric SIC has been investigated by using 14 mm circular shaped electrodes on both sides with the active mass loading of nearly 3 mg in each electrode. On the other hand, the electrodes were sized into 2 X 2 cm^2 for the pouch cell assembly. After filling the electrolyte into the pouch, the pouch was carefully sealed using the sealing machine inside the glove box.

The as-fabricated coin and pouch type symmetric cells were subjected to CV study at a scan rate of 20 mV s^{-1} to optimize the voltage window of the system (Supplementary figure S6 (a and b)). It is observed that when the potential exceeds 2.5 V, both the configurations show a sharp edge in the curve, which could be correlated with the decomposition of the components of the electrolyte. As a result, the maximum cell potential is limited to 2.5 V in order to cycle the cell under safer conditions. CV curves of both the configurations show similar trend and the CV curves indicate the formation of EDLC on the surface of CSC electrode. The formation of double layer in the symmetric configuration is due to the adsorption/de-sorption. i.e., both cations (Na^+) and anions (ClO^{4-}) contribute to the formation of the double layer in the case of symmetric configuration.

In order to estimate the capacitance of the symmetric cell in the chosen type of cell assembly, *viz.*, coin and pouch cell, galvanostatic charge-discharge (GCD) behaviour was studied individually in the potential window of 0.0 to 2.5 V at 1000 mA g^{-1} condition (Figure S7). GCD profile shows a linear variation with respect to the chosen potential window (0.0 - 2.5 V) and confirms that the storage behavior is mainly due to the double layer formation.

In the case of coin type cell, the maximum specific capacitance achieved is about 126.7 F g^{-1} at a current rate of 2 mA (0.325 mA g^{-1}). GCD profile of the coin type symmetric SIC, tested at different current rates is shown in figure 6a. The cell delivers a specific capacitance of 50.28 F g^{-1} at a maximum current rate of 15 mA (2.435 A g^{-1}), which is the maximum current rate used to test the performance of the cell in the present study. At this maximum current density, the discharge time is > 10 sec. Such an observation leads to an interference that CSC based cells of the present study could be tested beyond this current rate also, due to the observed discharge time limit (> 10 sec); because, supercapacitors are generally recommended for use in the range of fraction of seconds also in some specific applications. In parallel, the pouch cell was also tested at different current densities ranging from 4 (0.5 A g^{-1}) to 20 mA (2.5 A g^{-1}). GCD profile of the pouch type symmetric SIC tested at different current rates is shown in figure 6b. The cell delivers a maximum specific capacitance of 108 F g^{-1} at 0.5 A g^{-1}. The cell also delivers an appreciable specific capacitance of 28 F g^{-1} at 2.5 A g^{-1}. Capacitance of the cell calculated at different currents is given in figure 6c wherein pouch cell performance is found to have closer resemblance with that of the behavior of coin cell assembly. Details of specific capacitance values obtained at different current densities are given in Table S2 and S3 as a function of coin and pouch cell respectively. From the figure (6c) and from the table, it is evident that the pouch cell shows a specific capacitance of 108 F g^{-1} at 0.5 A g^{-1}, which is comparable with that of the coin type cell (127 F g^{-}

[1] at 0.3 A g^{-1}). Herein, difference observed in capacity values may be related to the engineering issues, leading to improper contact to support the EDLC behavior throughout the cycling study, which is applicable to pouch cell. Similar behavior is observed with the impedance spectral analysis of the pouch cell also which is discussed in view of stability factor.

Cycling stability is another important property of SICs. In the current study, both the cells were subjected to a high current rate (1000 mA g^{-1}) individually. The obtained profile of coin and pouch type cells is shown in figure 6d in combination with the Coulombic efficiency of the cells. It is evident that the cycle life of the coin cell shows slight fluctuation in behavior with the capacitance retention (when compared with its initial cycle) of more than 65 % and a Coulombic efficiency above 95% at the 300th cycle. On the other hand, cycle life of the pouch cell (figure 6f) tested at 1000 mA g^{-1} shows a steady performance, especially after 10 cycles. The pouch cell shows excellent capacitance retention even after 300 cycles, which is about 68%. The Coulombic efficiency of the pouch cell after 300 cycles is maintained above 95%. Further, cycling stability of the pouch cell device has been tested for 1000 cycles and the result is appended in figure S8. Retention of capacitance is found to decreases to 50% at the 1000th cycle; however, the observed fade in capacitance is found to be significant especially after 300 cycles, which in turn could be correlated to the unavoidable lack of material stability that occurs after 300 cycles. Based on the acceptable fade observed after prolonged cycling, the synthesised CSC electrode material is designated to be suitable for the Na-ion storage application, particularly in Na-ion capacitor. To substantiate the suitability factor, Nyquist plot of the as-fabricated cells and the cells after cycling is shown in figure 6e. The as-fabricated coin cell shows smaller charge transfer resistance of 8 Ω; this value is smaller than the one obtained for pouch cell (15 Ω). This may be due to the contact issue between the (comparatively) large area pouch cell components. The obtained charge transfer

resistance in both the cases are smaller (8 fold in coin cell and 4 fold in pouch) than the reported value (60 Ω) found in the literature for the citrus peel derived activated carbon based symmetric SIC[6]. After cycling, the charge transfer resistance increases and the impedance plot shows exactly the same trend in both the cell configurations. Such an observation may be due to the unavoidable and insignificant structural changes of CSC during charge/discharge process. The practical feasibility of the fabricated SIC as an energy storage system is successfully demonstrated by lighting the blue LED for 2 minutes (figure 6f) and running a clock for 25 minutes. Further, for the demonstration of sustainable lighting by blue LEDs, two pouch cells were connected in series to fulfill the required voltage. The recorded video is given as supplementary video.

Specific energy and power of the symmetric coin and pouch cells are estimated and included in the Ragone plot, wherein comparison of the pouch and coin cell configurations is shown (figure 7). It is to be noted that the coin cell delivers a maximum specific energy of 109 Wh kg^{-1} at a power of 1.6 kW kg^{-1}; whereas the cell delivers a maximum power of about 12.16 kW/kg at an energy density of 43.57 Wh kg^{-1}. In the case of pouch cell, the maximum specific energy and power are 116 Wh kg^{-1} (corresponding specific power is 1.56 kW kg^{-1}) and 7.8 kW kg^{-1} (corresponding specific energy 30 Wh kg^{-1}). These values are comparable in general and superior in certain cases with respect to the literature reported values of Na-ion capacitor and the comparison of performance is shown in Table S3[6, 46-53].

With a view to understand the cycling stability and tolerance limit of CSC electrode as a function of cell design leakage test has been performed individually. Figure S9 displays the self-discharge curves of devices charged to 2.5 V potential (at 2 mA current condition) wherein one could observe that the pouch cell shows increasing self-discharge behavior due to the likely to be poor contact between the electrodes, attributable to the lack of pouch cell fabrication facility. Leakage current

of the devices is calculated by, $I_{leak} = C\frac{dv}{dt}$. where, C is capacitance, v is voltage and t is time. The calculated leakage current from the slope of voltage vs. time plot is 34.7 and 54 µA for coin and pouch cell respectively. Further studies are in progress to improve the specific energy and power of the material under investigation, especially at high current conditions, and the cycling stability in both the coin and pouch cell configurations by modifying the surface structure of the CSC material.

CONCLUSION

Corn silk derived carbon (CSC) with KOH activation demonstrates itself as a suitable electrode material for sodium ion storage applications. Microporous CSC, owing its specific surface area of 2550 m^2 g^{-1} along with the adequate pore volume of 0.95 cm^3 g^{-1} is capable of accommodating sodium ions. CSC electrode based half-cell configuration cycled between 1.5 to 4.2 V potential region stores sodium ions at the surface of carbon and delivers a capacity of 265 mA h g^{-1} at 100 mA g^{-1}. In addition, CSC electrodes were tested in a symmetric cell configuration in the form of coin and pouch cell assembly. Of the two configurations, maximum specific energy density of 109 Wh kg^{-1} (0.324 A g^{-1}) and a power density of 12.16 kW kg^{-1} (at 2.5 A g^{-1}) are achieved at different current density conditions deployed for the coin cell system. The practical feasibility of the fabricated SIC as an energy storage system has been successfully demonstrated by lighting the blue LED for 2 minutes and running a clock for 25 minutes. The superior storage behavior of CSC electrode in sodium ion capacitor could be attributed to the larger specific surface area, microporous nature of carbon, presence of nitrogen and the suitable pore volume, which are the key factors responsible to accommodating more number of sodium ions in its structure. This work showcases a new route to develop sodium ion capacitors using a reusable activated carbon derived from the bio waste, bestowed with low cost benefits.

METHODS

Materials

All chemicals were purchased from Sigma Aldrich and were used without further purification. Corn silk was collected from corn, purchased from a local market. Triple distilled water was used for all the experiments.

Synthesis of Corn silk derived carbon (CSC)

Corn silk collected from corn was washed with DI water followed by ethanol rinsing to remove impurities and dried at 80° C. The above dried material was crushed with the help of mortar and pestle. Then the powder was subjected to pre-carbonization under the influence of argon (Ar) flow and heat treated at 350° C for 2h with 2° C min^{-1} ramping. 1 g of pre-carbonized material (denoted as CS-350) was ground well with 2 g of KOH and heated at 800° C for 2h in Ar atmosphere with a heating rate of 5° C min^{-1}. The obtained foam kind of black product was ground and the powder was washed with 1 M HCl solution repeatedly to remove the metal impurities. The material was further washed with triple distilled water many times till it reaches the neutral pH and dried finally at 80° C in vacuum, to get the desired product and is denoted as CSC and the yield of the product is nearly 25-30%.

Physical and electrochemical characterization

Phase purity of synthesized CSC was characterized by powder diffraction technique using PANalytical X'pert PRO diffractometer with Ni-filtered Cu-Kα radiation and the data was analyzed between 2Θ=10-80° with a scan rate of 5° min^{-1}. Raman spectrum was recorded using a BRUKER RFS 27 stand alone FT-Raman spectrometer in the 300–4000 cm^{-1} spectral range and the laser source is Nd:YAG 1064 nm. The electrical conductivity of CSC was calculated by using four probe technique with SES Instrument Pvt, Ltd. Morphology

of CSC is investigated from scanning electron microscope (JEOL 6701F), Gemini Field Emission Scanning Electron Microscopy (FE-SEM) Tecnai 20 G2 (FEI make) and High Resolution Transmission Electron Microscopy (HR-TEM) images were captured from Jeol Jem 2100 TEM analyzer. Elemental analysis (EDAX) was carried out by using Elementar Model Vario EL III. XPS (X-ray photoelectron Spectroscopy) spectra were recorded from MULTILAB 2000 base system with an excitation source of Mg Kα radiation. All the electrochemical studies were carried out using Biologic electrochemical workstation and ARBIN cycler.

Electrode Fabrication

The as-prepared electrodes include a mixture of 80:10:10 wt. % of active material, super P carbon and polyvinylidene diflouride (PVdF) binder respectively. N-methyl pyrrolidone (NMP) was used as a solvent to dissolve the PVdF polymer present in the mixture. The solvent added mixture was continuously ground to obtain a homogenous slurry. Subsequently, the slurry was coated on aluminium and copper foil (current collector) separately, dried under vacuum at 80° C for 12 h and pressed with 3 ton pressure. Such a hot roll pressed electrode was cut into circular shape (14 mm) and the electrodes typically had an active material content of ~3 mg (The material loading of CSC is approximately ~1.5 mg cm^{-2}). The electrode was further dried under vacuum at 80° C for 30 min, prior to the assembling of cells in an argon-filled glove box and hermetically sealed after cell fabrication using crimp sealing machine. Electrochemical characterization was carried out on freshly fabricated 2032 coin cells consisting of CSC electrodes and a non-aqueous electrolyte containing 1M NaClO4 (dissolved in 1:1 v/v EC:PC) along with polypropylene as a separator.

SUPPORTING INFORMATION

Additional Figures S1 to S9 and Tables S1 to S4. This material is available free of charge via the Internet at http://pubs.acs.org.

XRD of CS-350, SEM images of corn silk at different stages of activation, EDAX, BET, Conductivity studies of CSC, CV curves, CDC profile, Cycling stability and Self-discharge studies of symmetric devices (Figures S1-S9) BET and Electrochemical performance details of symmetric coin cell and pouch cell devices (Tables S1-S3) Comparison of symmetric SIC pouch cell device performance with other reports (Table S4).

AUTHOR INFORMATION

Corresponding Author

* N.Kalaiselvi

E-mail: kalaiselvicecri@gmail.com

ACKNOWLEDGMENT

CSIR, New Delhi and DST, New Delhi are greatly acknowledged for financial support through MULTIFUN, GAP-14/16 and GAP-11/17 projects respectively.

REFERENCES

(1) Pan, H.; Hu, Y.-S.; Chen, L. Room-temperature stationary sodium-ion batteries for large-scale electric energy storage. *Energy & Environmental Science* **2013,** *6* (8), 2338-2360.

(2) Slater, M. D.; Kim, D.; Lee, E.; Johnson, C. S. Sodium-Ion Batteries. *Advanced Functional Materials* **2013,** *23* (8), 947-958.

(3) Liu, S.; Cai, Z.; Zhou, J.; Pan, A.; Liang, S. Nitrogen-doped TiO2 nanospheres for advanced sodium-ion battery and sodium-ion capacitor applications. *Journal of Materials Chemistry A* **2016,** *4* (47), 18278-18283.

(4) Ajuria, J.; Redondo, E.; Arnaiz, M.; Mysyk, R.; Rojo, T.; Goikolea, E. Lithium and sodium ion capacitors with high energy and power densities based on carbons from recycled olive pits. *Journal of Power Sources* **2017,** *359*, 17-26.

(5) Yun Young, S.; Cho Se, Y.; Kim, H.; Jin, H.-J.; Kang, K. Ultra-Thin Hollow Carbon Nanospheres for Pseudocapacitive Sodium-Ion Storage. *ChemElectroChem* **2014,** *2* (3), 359-365,.

(6) Kim, N. R.; Yun, Y. S.; Song, M. Y.; Hong, S. J.; Kang, M.; Leal, C.; Park, Y. W.; Jin, H.-J. Citrus-Peel-Derived, Nanoporous Carbon Nanosheets Containing Redox-Active Heteroatoms for Sodium-Ion Storage. *ACS Applied Materials & Interfaces* **2016,** *8* (5), 3175-3181.

(7) Jian, Z.; Raju, V.; Li, Z.; Xing, Z.; Hu, Y.-S.; Ji, X. A High-Power Symmetric Na-Ion Pseudocapacitor. *Advanced Functional Materials* **2015,** *25* (36), 5778-5785.

(8) Wang, Y.; Song, Y.; Xia, Y. Electrochemical capacitors: mechanism, materials, systems, characterization and applications. *Chemical Society Reviews* **2016,** *45* (21), 5925-5950.

(9) Zhong, C.; Deng, Y.; Hu, W.; Qiao, J.; Zhang, L.; Zhang, J. A review of electrolyte materials and compositions for electrochemical supercapacitors. *Chemical Society Reviews* **2015,** *44* (21), 7484-7539.

(10) Chmiola, J.; Yushin, G.; Gogotsi, Y.; Portet, C.; Simon, P.; Taberna, P. L. Anomalous Increase in Carbon Capacitance at Pore Sizes Less Than 1 Nanometer. *Science* **2006,** *313* (5794), 1760.

(11) Wang, L.; Schnepp, Z.; Titirici, M. M. Rice husk-derived carbon anodes for lithium ion batteries. *Journal of Materials Chemistry A* **2013,** *1* (17), 5269-5273.

(12) Zhang, F.; Wang, K.-X.; Li, G.-D.; Chen, J.-S. Hierarchical porous carbon derived from rice straw for lithium ion batteries with high-rate performance. *Electrochemistry Communications* **2009,** *11* (1), 130-133.

(13) Arrebola, J. C.; Caballero, A.; Hernán, L.; Morales, J.; Olivares-Marín, M.; Gómez-Serrano, V. Improving the Performance of Biomass-Derived Carbons in Li-Ion Batteries by Controlling the Lithium Insertion Process. *Journal of The Electrochemical Society* **2010,** *157* (7), A791-A797.

(14) Caballero, A.; Hernán, L.; Morales, J. Limitations of Disordered Carbons Obtained from Biomass as Anodes for Real Lithium-Ion Batteries. *ChemSusChem* **2011,** *4* (5), 658-663.

(15) Saravanan, K. R.; Mullaivananathan, V.; Kalaiselvi, N. Dual hetero atom containing bio-carbon: Multifunctional electrode material for High Performance Sodium-ion Batteries and Oxygen Reduction Reaction. *Electrochimica Acta* **2015,** *176*, 670-678.

(16) Sun, L.; Tian, C.; Li, M.; Meng, X.; Wang, L.; Wang, R.; Yin, J.; Fu, H. From coconut shell to porous graphene-like nanosheets for high-power supercapacitors. *Journal of Materials Chemistry A* **2013,** *1* (21), 6462-6470.

(17) Wei, L.; Yushin, G. Electrical double layer capacitors with activated sucrose-derived carbon electrodes. *Carbon* **2011,** *49* (14), 4830-4838.

(18) Genovese, M.; Jiang, J.; Lian, K.; Holm, N. High capacitive performance of exfoliated biochar nanosheets from biomass waste corn cob. *Journal of Materials Chemistry A* **2015,** *3* (6), 2903-2913.

(19) Mullaivananathan, V.; Sathish, R.; Kalaiselvi, N. Coir Pith Derived Bio-carbon: Demonstration of Potential Anode Behavior in Lithium-ion Batteries. *Electrochimica Acta* **2017,** *225*, 143-150.

(20) Mullaivananathan, V.; Packiyalakshmi, P.; Kalaiselvi, N. Multifunctional bio carbon: a coir pith waste derived electrode for extensive energy storage device applications. *RSC Advances* **2017,** *7* (38), 23663-23670.

(21) Ding, J.; Wang, H.; Li, Z.; Cui, K.; Karpuzov, D.; Tan, X.; Kohandehghan, A.; Mitlin, D. Peanut shell hybrid sodium ion capacitor with extreme energy-power rivals lithium ion capacitors. *Energy & Environmental Science* **2015,** *8* (3), 941-955.

(22) Oda, H.; Yamashita, A.; Minoura, S.; Okamoto, M.; Morimoto, T. Modification of the oxygen-containing functional group on activated carbon fiber in electrodes of an electric double-layer capacitor. *Journal of Power Sources* **2006,** *158* (2), 1510-1516.

(23) Yan, X.; Yu, Y.; Yang, X. Effects of electrolytes on the capacitive behavior of nitrogen/phosphorus co-doped nonporous carbon nanofibers: an insight into the role of phosphorus groups. *RSC Advances* **2014,** *4* (48), 24986-24990.

(24) Hulicova, D.; Kodama, M.; Hatori, H. Electrochemical Performance of Nitrogen-Enriched Carbons in Aqueous and Non-Aqueous Supercapacitors. *Chemistry of Materials* **2006,** *18* (9), 2318-2326.

(25) Hulicova-Jurcakova, D.; Puziy, A. M.; Poddubnaya, O. I.; Suárez-García, F.; Tascón, J. M. D.; Lu, G. Q. Highly Stable Performance of Supercapacitors from Phosphorus-Enriched Carbons. *Journal of the American Chemical Society* **2009,** *131* (14), 5026-5027.

(26) Dong, S.; Chen, X.; Zhang, X.; Cui, G. Nanostructured transition metal nitrides for energy storage and fuel cells. *Coordination Chemistry Reviews* **2013,** *257* (13), 1946-1956.

(27) Yang, Z.; Guo, H.; Li, X.; Wang, Z.; Yan, Z.; Wang, Y. Natural sisal fibers derived hierarchical porous activated carbon as capacitive material in lithium ion capacitor. *Journal of Power Sources* **2016,** *329*, 339-346.

(28) Yan, J.; Cao, W. J.; Zheng, J. P. Constructing High Energy and Power Densities Li-Ion Capacitors Using Li Thin Film for Pre-Lithiation. *Journal of The Electrochemical Society* **2017,** *164* (9), A2164-A2170.

(29) Cao, W. J.; Luo, J. F.; Yan, J.; Chen, X. J.; Brandt, W.; Warfield, M.; Lewis, D.; Yturriaga, S. R.; Moye, D. G.; Zheng, J. P. High Performance Li-Ion Capacitor Laminate Cells Based on Hard Carbon/Lithium Stripes Negative Electrodes. *Journal of The Electrochemical Society* **2017,** *164* (2), A93-A98.

(30) Rahman, N. A.; Wan Rosli, W. I. Nutritional compositions and antioxidative capacity of the silk obtained from immature and mature corn. *Journal of King Saud University - Science* **2014,** *26* (2), 119-127.

(31) Hasanudin, K.; Hashim, P.; Mustafa, S. Corn Silk (Stigma Maydis) in Healthcare: A Phytochemical and Pharmacological Review. *Molecules* **2012,** *17* (8).

(32) Wan, W.; Wang, Q.; Zhang, L.; Liang, H.-W.; Chen, P.; Yu, S.-H. N-, P- and Fe-tridoped nanoporous carbon derived from plant biomass: an excellent oxygen reduction electrocatalyst for zinc-air batteries. *Journal of Materials Chemistry A* **2016,** *4* (22), 8602-8609.

(33) Pan, D.; Wang, S.; Zhao, B.; Wu, M.; Zhang, H.; Wang, Y.; Jiao, Z. Li Storage Properties of Disordered Graphene Nanosheets. *Chemistry of Materials* **2009,** *21* (14), 3136-3142.

(34) Ferrari, A. C.; Robertson, J. Interpretation of Raman spectra of disordered and amorphous carbon. *Physical Review B* **2000,** *61* (20), 14095-14107.

(35) Ou, J.; Zhang, Y.; Chen, L.; Zhao, Q.; Meng, Y.; Guo, Y.; Xiao, D. Nitrogen-rich porous carbon derived from biomass as a high performance anode material for lithium ion batteries. *Journal of Materials Chemistry A* **2015,** *3* (12), 6534-6541.

(36) Luo, W.; Schardt, J.; Bommier, C.; Wang, B.; Razink, J.; Simonsen, J.; Ji, X. Carbon nanofibers derived from cellulose nanofibers as a long-life anode material for rechargeable sodium-ion batteries. *Journal of Materials Chemistry A* **2013,** *1* (36), 10662-10666.

(37) Ferrero, G. A.; Fuertes, A. B.; Sevilla, M. N-doped porous carbon capsules with tunable porosity for high-performance supercapacitors. *Journal of Materials Chemistry A* **2015,** *3* (6), 2914-2923.

(38) Mao, L.; Zhang, Y.; Hu, Y.; Ho, K. H.; Ke, Q.; Liu, H.; Hu, Z.; Zhao, D.; Wang, J. Activation of sucrose-derived carbon spheres for high-performance supercapacitor electrodes. *RSC Advances* **2015,** *5* (12), 9307-9313.

(39) Wei, L.; Sevilla, M.; Fuertes Antonio, B.; Mokaya, R.; Yushin, G. Polypyrrole-Derived Activated Carbons for High-Performance Electrical Double-Layer Capacitors with Ionic Liquid Electrolyte. *Advanced Functional Materials* **2011,** *22* (4), 827-834.

(40) López, G. P.; Castner, D. G.; Ratner, B. D. XPS O 1s binding energies for polymers containing hydroxyl, ether, ketone and ester groups. *Surface and Interface Analysis* **1991,** *17* (5), 267-272.

(41) Chen, Z.; Dahn, J. R. Reducing Carbon in LiFePO4 / C Composite Electrodes to Maximize Specific Energy, Volumetric Energy, and Tap Density. *Journal of The Electrochemical Society* **2002,** *149* (9), A1184-A1189.

(42) Kim, M.-S.; Kim, H.-K.; Lee, S.-W.; Kim, D.-H.; Ruan, D.; Chung, K. Y.; Lee, S. H.; Roh, K. C.; Kim, K.-B. Synthesis of Reduced Graphene Oxide-Modified LiMn0.75Fe0.25PO4 Microspheres by Salt-Assisted Spray Drying for High-Performance Lithium-Ion Batteries. *Scientific Reports* **2016,** *6*, 26686.

(43) Yin, S.; Zhang, Y.; Kong, J.; Zou, C.; Li, C. M.; Lu, X.; Ma, J.; Boey, F. Y. C.; Chen, X. Assembly of Graphene Sheets into Hierarchical Structures for High-Performance Energy Storage. *ACS Nano* **2011,** *5* (5), 3831-3838.

(44) Flandrois, S.; Simon, B. Carbon materials for lithium-ion rechargeable batteries. *Carbon* **1999,** *37* (2), 165-180.

(45) Ali, G.; Mehmood, A.; Ha, H. Y.; Kim, J.; Chung, K. Y. Reduced graphene oxide as a stable and high-capacity cathode material for Na-ion batteries. *Scientific Reports* **2017,** *7*, 40910.

(46) Jain, A.; Jayaraman, S.; Ulaganathan, M.; Balasubramanian, R.; Aravindan, V.; Srinivasan, M. P.; Madhavi, S. Highly mesoporous carbon from Teak wood sawdust as prospective electrode for the construction of high energy Li-ion capacitors. *Electrochimica Acta* **2017,** *228*, 131-138.

(47) Chen, J.; Zhou, X.; Mei, C.; Xu, J.; Zhou, S.; Wong, C.-P. Evaluating biomass-derived hierarchically porous carbon as the positive electrode material for hybrid Na-ion capacitors. *Journal of Power Sources* **2017,** *342*, 48-55.

(48) Wang, H.; Mitlin, D.; Ding, J.; Li, Z.; Cui, K. Excellent energy-power characteristics from a hybrid sodium ion capacitor based on identical carbon nanosheets in both electrodes. *Journal of Materials Chemistry A* **2016,** *4* (14), 5149-5158.

(49) Yun, Y. S.; Cho, S. Y.; Kim, H.; Jin, H.-J.; Kang, K. Ultra-Thin Hollow Carbon Nanospheres for Pseudocapacitive Sodium-Ion Storage. *ChemElectroChem* **2015,** *2* (3), 359-365.

(50) Yin, J.; Qi, L.; Wang, H. Sodium Titanate Nanotubes as Negative Electrode Materials for Sodium-Ion Capacitors. *ACS Applied Materials & Interfaces* **2012,** *4* (5), 2762-2768.

(51) Chen, Z.; Augustyn, V.; Jia, X.; Xiao, Q.; Dunn, B.; Lu, Y. High-Performance Sodium-Ion Pseudocapacitors Based on Hierarchically Porous Nanowire Composites. *ACS Nano* **2012,** *6* (5), 4319-4327.

(52) Ding, R.; Qi, L.; Wang, H. An investigation of spinel NiCo2O4 as anode for Na-ion capacitors. *Electrochimica Acta* **2013,** *114*, 726-735.

(53) Zhao, L.; Qi, L.; Wang, H. Sodium titanate nanotube/graphite, an electric energy storage device using Na+-based organic electrolytes. *Journal of Power Sources* **2013,** *242*, 597-603.

FIGURES

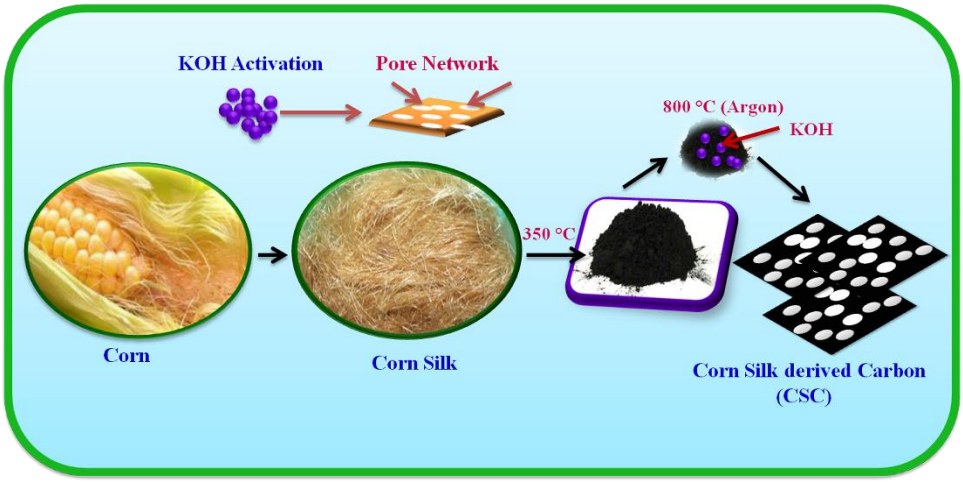

Figure 1. Schematic illustration of synthesis of Corn silk derived carbon (CSC)

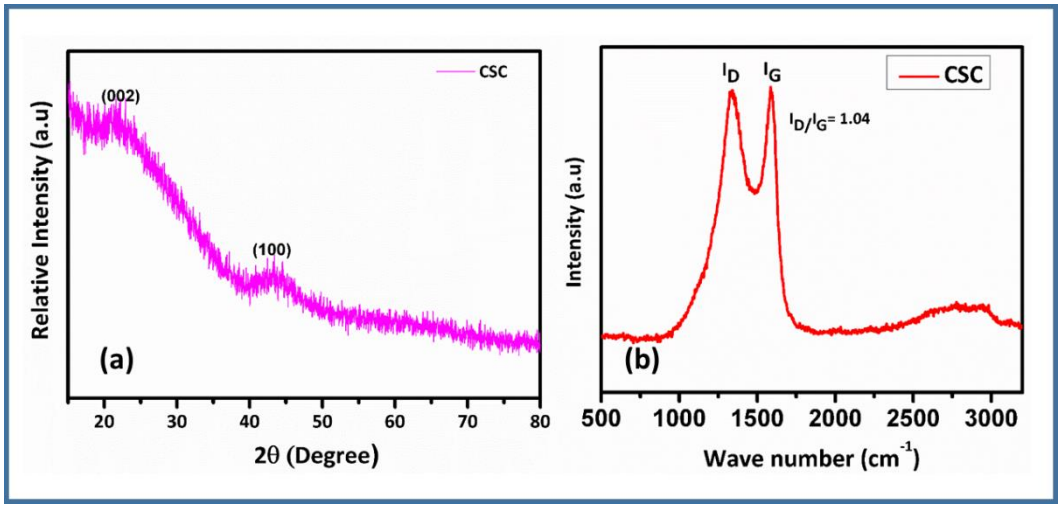

Figure 2. XRD and Raman spectrum of currently synthesized CSC

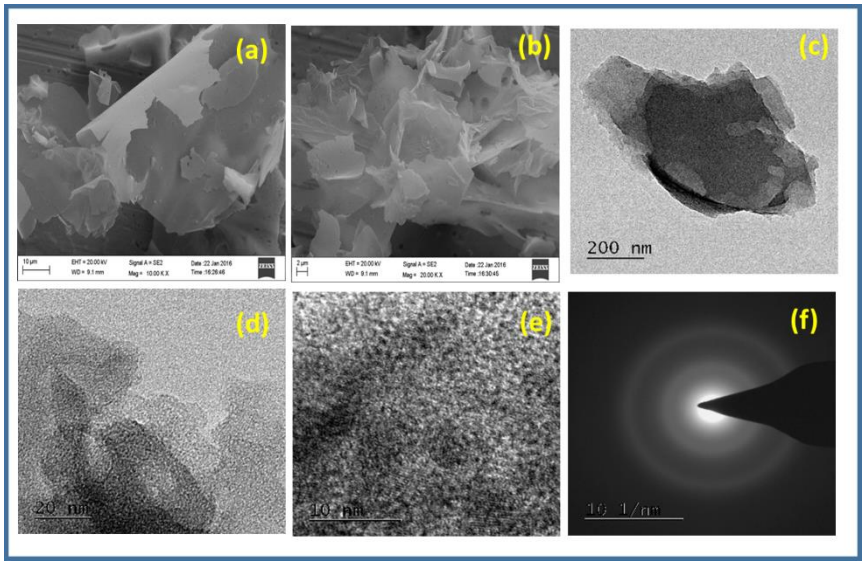

Figure 3. (a, b) FESEM images (c-e) HRTEM images and (f) SAED pattern of synthesized CSC electrode material

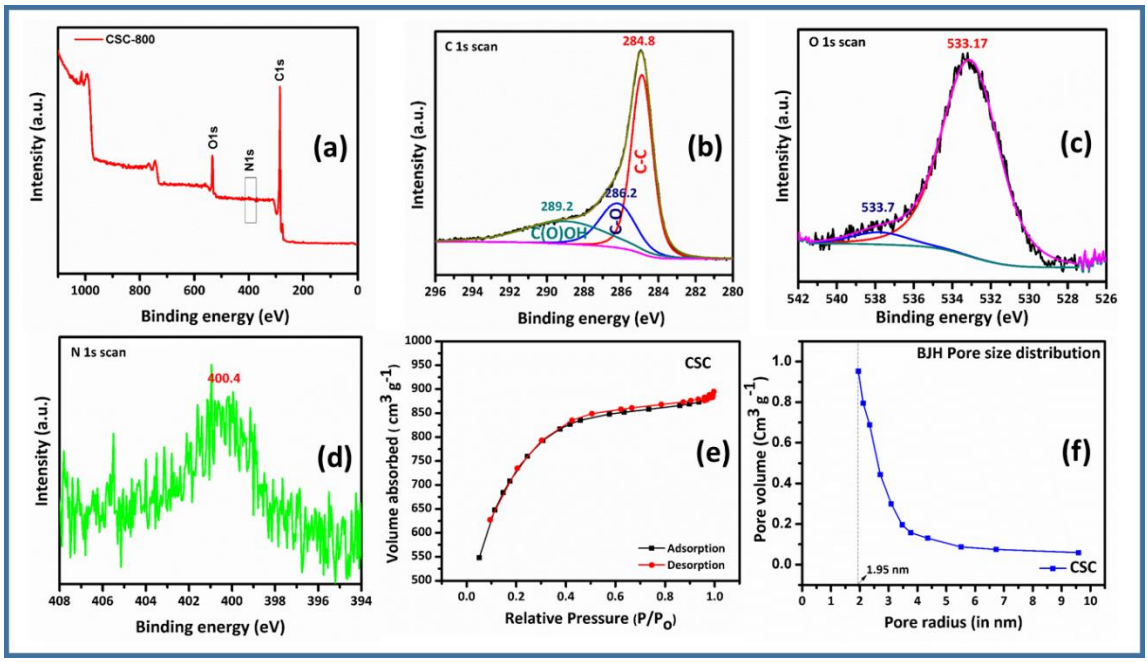

Figure 4. XPS and BET analysis of CSC (a) survey spectrum, (b-d) corresponding to C1s, O1s, N1s scan, (e) N_2 adsorption isotherm and (f) BJH pore size distribution

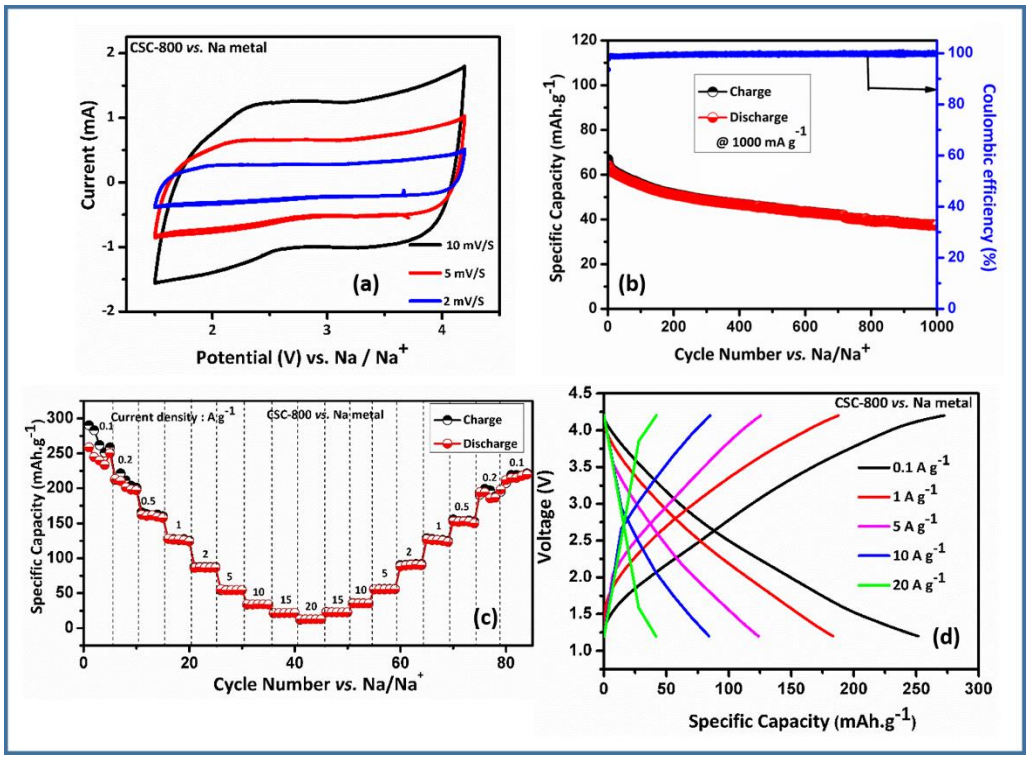

Figure 5. (a) CV curves of CSC in the 1.5 and 4.2 V potential region recorded at different scan rates vs. Na/Na^+ (b) CDC studies of CSC *vs.* sodium metal at a current density of 1000 mA g^{-1} (c) Rate capability studies of CSC electrode and (d) CDC profile of CSC obtained from rate capability studies

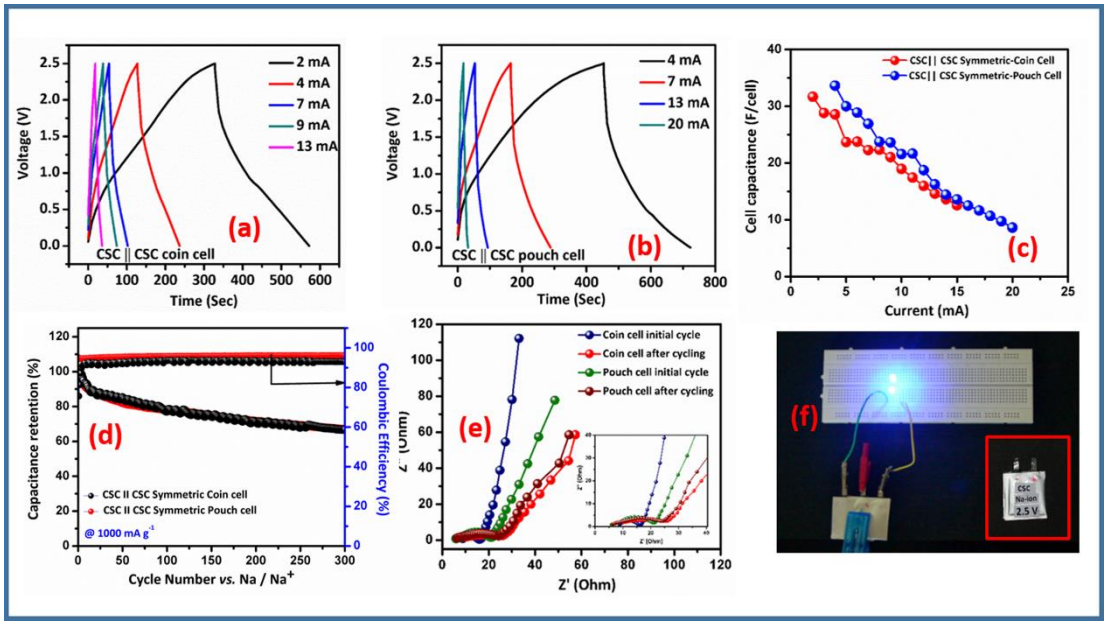

Figure 6. Electrochemical performance of symmetric CSC coin and pouch cell devices in the potential window 0.01 to 2.5 V in 1 M $NaClO_4$ dissolved in EC/PC (1:1 v/v) electrolyte **(**a, b) galvanostatic charge-discharge profile of CSC at various current (c) Rate capability studies of CSC electrode and (d) Cycling performance of symmetric CSC devices (e) EIS spectroscopy of symmetric devices corresponding to initial and after cycled at 1000 mA g^{-1} current density (f) Demonstration of pouch cell device

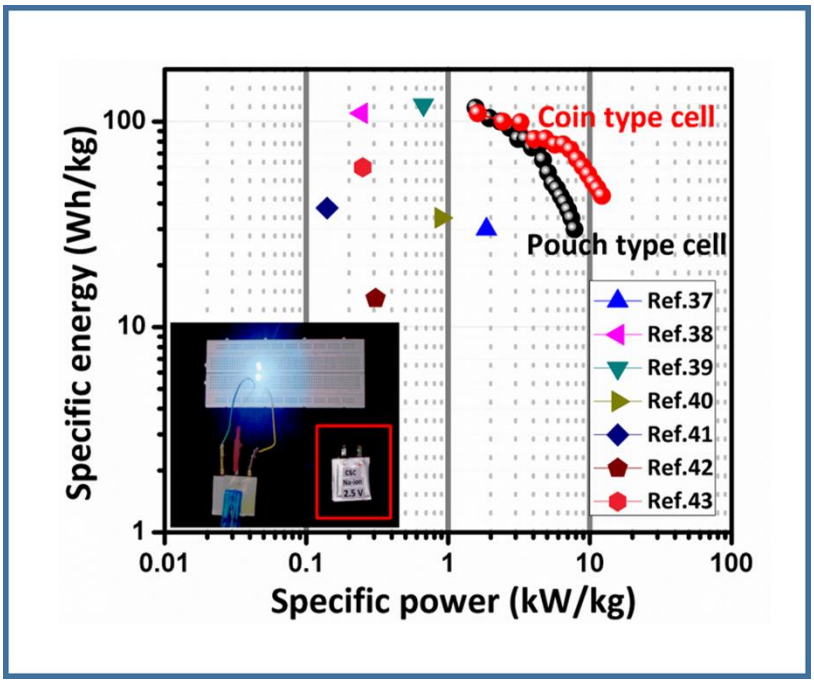

Figure 7. Ragone plot indicating the performance of symmetric (a) coin and (b) pouch cell device versus reported behavior of state-of-the-art (Ref. 37-43) sodium-ion capacitors

Table of Contents Graphic and Synopsis

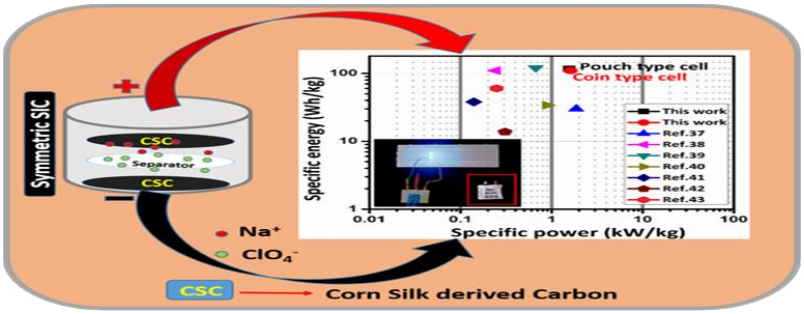

This work demonstrates the performance of sodium ion capacitors containing bio waste driven cost effective activated carbon.

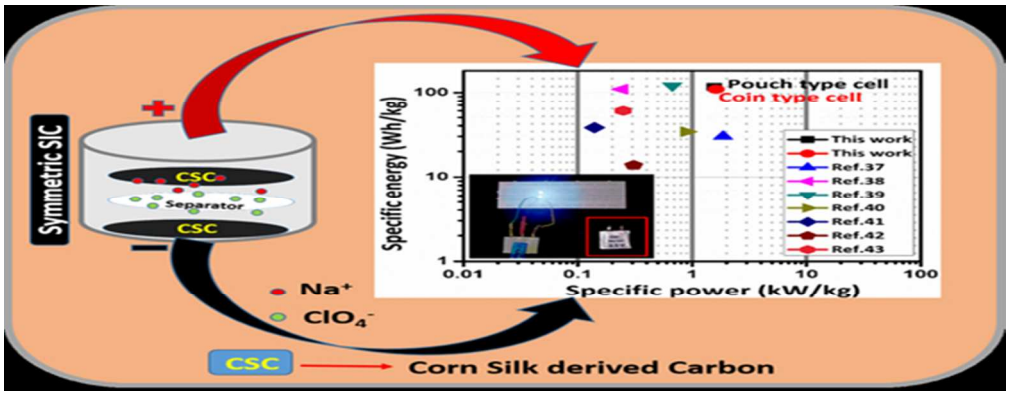

This work demonstrates the performance of sodium ion capacitors containing bio waste driven cost effective activated carbon

130x50mm (150 x 150 DPI)